Available online at www.sciencedirect.com
ScienceDirect
Journal of the European Ceramic Society 31 (2011) 589–596
www.elsevier.com/locate/jeurceramsoc

Low temperature sintering of barium titanate based ceramics with high dielectric constant for LTCC applications

Hamid Naghib-zadeh *, Carsten Glitzky, Werner Oesterle, Torsten Rabe

Federal Institute for Materials Research and Testing, 12203 Berlin, Germany

Received 1 June 2010; received in revised form 30 September 2010; accepted 3 October 2010
Available online 20 November 2010

Abstract

The sintering temperature of $BaTiO_3$ powder was reduced to 900 °C due to the $ZnO–B_2O_3–Li_2O–Nb_2O_5–Co_2O_3$ addition. Excellent densification was achieved after sintering at 900 °C for 2 h. The low sintering temperature of newly developed capacitor materials allows a co-firing with pure silver electrodes. The dielectric constant and the temperature stability of the dielectric constant are strongly correlated with the composition of the $ZnO–B_2O_3–Li_2O$ additives. A high dielectric constant up to 3000 and a dielectric loss less than 0.024 were measured on multilayer capacitors sintered at 900 °C with silver inner electrodes.

Keywords: $BaTiO_3$ and titanates; Capacitors; Dielectric properties; LTCC

1. Introduction

Low temperature co-fired ceramics (LTCC) must be sintered at temperatures below 900 °C which allows the use of low resistivity and low cost silver conductors. Integration of passive components such as capacitors into the LTCC module eliminates many solder joints and wire bonds and is required for the miniaturization of electronic packaging. However, commercially available barium titanate based ceramic powders, which are mostly used for capacitor manufacturing are sintered at temperatures above 1000 °C. Hence, it is required to develop capacitor materials which can be fully densified at a sintering temperature below 900 °C.

In general, there are several methods to lower the sintering temperature of ceramics, such as addition of glasses or oxides as sintering aids, chemical processing and using smaller particle size of the starting materials.[1] In this paper, the addition of sintering aids as the more commonly used method is discussed.

Many authors have investigated the low-temperature sintering of $BaTiO_3$-based ceramics.[2] Various types of sintering aids, such as LiF-containing additives,[3,4] Li_2O-containing additives,[5] several borosilicate glass powders,[6,7] $ZnO–B_2O_3$, $CdO–B_2O_3$, $CaO–B_2O_3$, $Bi_2O_3–B_2O_3$[8,9] and $CaO–Al_2O_3–B_2O_3$ compositions[10] have been used to decrease the sintering temperature of $BaTiO_3$. However, the addition of sintering aids often results in the degradation of dielectric properties of $BaTiO_3$. Therefore, the choice of a suitable sintering aid composition which can reduce the sintering temperature below 900 °C without deterioration of dielectric properties of the host material is important. The desirable dielectric properties include a high and almost temperature-independent dielectric constant and a low dielectric loss.

In order to achieve a high dielectric constant, it is important that the sintered body is as free as possible from low-dielectric-constant second phases. A key step is to find sintering aid compositions that permit limited grain growth during sintering. During grain growth, certain ions from the low melting phase were found to be incorporated into the barium titanate lattice modifying the ceramic properties and reducing the volume fraction of the low-dielectric-constant phase.[8]

The flux systems in this study were chosen from combinations of B_2O_3 with modifiers such as Li_2O and ZnO because of many low melting compositions containing these compounds and partially solubility of Li_2O and ZnO modifiers in barium titanate perovskite.[8] Nb_2O_5 and Co_2O_3 were added to improve the dielectric properties. We investigated the influence

* Corresponding author. Tel.: +49 3081044442.
E-mail address: h55zadeh@yahoo.com (H. Naghib-zadeh).

0955-2219/$ – see front matter © 2010 Elsevier Ltd. All rights reserved.
doi:10.1016/j.jeurceramsoc.2010.10.003

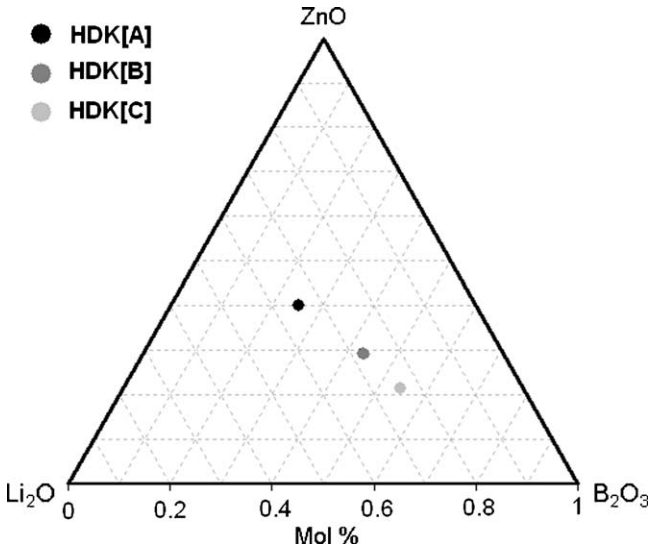

Fig. 1. Composition of $ZnO–B_2O_3–Li_2O$ flux in HDK[A], HDK[B] and HDK[C].

of $ZnO–B_2O_3–Li_2O–Nb_2O_5–Co_2O_3$ compositions on the sintering behaviour and dielectric characteristics of commercially available $BaTiO_3$-powder.

2. Materials and methods

The starting powders were high-purity $BaTiO_3$ with an average particle size of 0.7 μm (ABT-O-21, Ferro Corp., Uden, Netherlands), ZnO (Chemapol, ≥99.5%, Prag, Czech Republic), Li_2CO_3 (UCB, ≥99%, Brussels, Belgium), B_2O_3 (Merk, ≥99.5%, Darmstadt, Germany), Nb_2O_5 (Roth, ≥99.9%, Karlsruhe, Germany) and Co_2O_3 (Alfa Aesar, ≥99.7%, Karlsruhe, Germany). Three different compositions from $ZnO–B_2O_3–Li_2O$ flux system (3.5 wt%) were chosen and mixed/milled for 3 h with barium titanate and 1.5 wt% pre-calcinated $Nb_2O_5–Co_3O_4$ (Nb:Co = 2:1) in ethanol by attrition milling (4V1M, Netzsch GmbH, Selb, Germany) using 2 mm diameter zirconium oxide balls. The dried powders were then uniaxially pressed and sintered at 900 °C for 2 h. The three new capacitor materials will be addressed in this work as HDK[A], HDK[B] and HDK[C]. B_2O_3-content in $ZnO–B_2O_3–Li_2O$ flux increases from HDK[A] to HDK[B] to HDK[C] while Li_2O- and ZnO-contents decrease (Fig. 1). For preparation of ceramic tapes, the prepared powders were mixed with suitable solvent, dispersant, plasticizer and binder for about 20 h to form a slurry. Tapes were then casted by doctor blade method. After screen printing of silver electrodes the tapes were stacked and laminated at 75 °C under 30 MPa pressure. The laminates were then debindered at 550 °C and subsequently sintered at 900 °C for 2 h in the air.

The coefficient of thermal expansion (CTE) and the shrinkage behaviours were measured using a dilatometer DIL802 (Bähr GmbH, Hüllhorst, Germany). The heating rates for dilatometric measurements were 5 K/min. Bulk density and open porosity were determined by Archimedes and water saturation methods.

XRD measurements were processed with PW 1710 powder diffractometer (Philips, Eindhoven, Netherlands). Microprobe analyses were carried out on a JXA-8900 RL (JEOL Ltd., Tokyo, Japan) electron microprobe. The microstructure of the samples was characterized by scanning electron microscopy (SEM, ZEISS Gemini Supra 40, Oberkochen, Germany) and transmission electron microscopy (JEM-2200FS, JEOL Ltd., Tokyo, Japan) equipped with energy dispersive X-ray (EDX) spectrometer for element analysis. TEM-specimen preparation was performed by focused ion beam technique (FIB, FEI Strata 200xP, Eindhoven, Netherlands). The dielectric properties were measured using an impedance analyser HP 4194A (Hewlett Packard Co., Santa Clara, CA, USA).

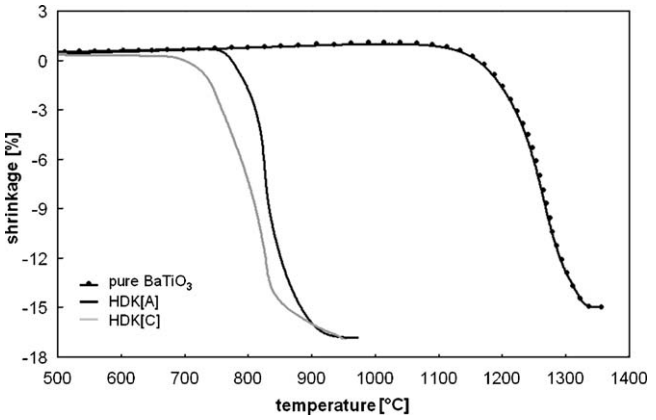

Fig. 2. Shrinkage behaviour of pure and additives containing $BaTiO_3$ measured with heating rate of 5 K/min.

3. Results and discussions

Fig. 2 shows the linear shrinkage of a pure $BaTiO_3$ sample compared to HDK[A] and HDK[C]. Pure $BaTiO_3$ starts to shrink at about 1100 °C and densification is completed at about 1340 °C while HDK[A] and HDK[C] start to shrink at about 750 °C and 700 °C, respectively, and densification is completed at about 940 °C. Additives containing $BaTiO_3$ samples can be densified at about 400 K below the sintering temperature of pure $BaTiO_3$.

The properties of sintered ceramics are listed in Table 1. Excellent densification and high dielectric constant were obtained for HDK[A] sintered at 900 °C for 2 h. The bulk density

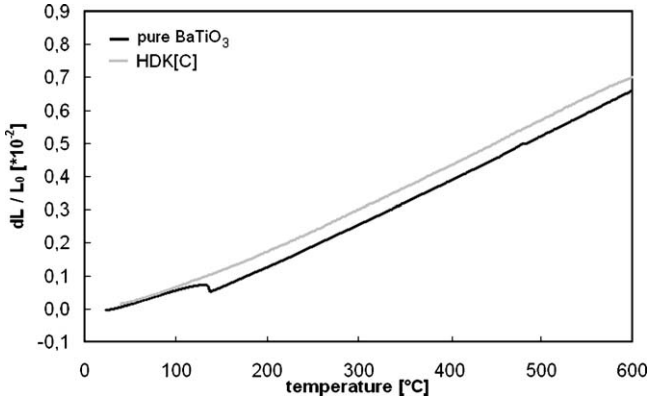

Fig. 3. CTE-curves of pure $BaTiO_3$ and HDK[C].

Table 1
Properties of pure and additive containing $BaTiO_3$ ceramics.

Samples	Additives [wt.%]	Sintering temperature [°C]	Open porosity [%]	Densification [%]	CTE (100–400 °C) [ppm/K]	ε_r (25 °C, 1 kHz)	tan δ (25 °C, 1 kHz)
Pure $BaTiO_3$	–	1300	0.8	98	11	2500	0.03
HDK[A]	5 (Zn–B–Li–Nb–Co–O)	900	0.8	98	–	2370	0.03
HDK[B]	5 (Zn–B–Li–Nb–Co–O)	900	3	94	–	1790	0.04
HDK[C]	5 (Zn–B–Li–Nb–Co–O)	900	5	93	12.3	1280	0.03

was 98% of the theoretical density and the dielectric constant (ε_r) was 2370. The densification and the dielectric constant decrease with the increasing of B_2O_3-content in ZnO–B_2O_3–Li_2O flux system from HDK[A] to HDK[B] to HDK[C]. For the uniaxially pressed samples of HDK[C] a densification of about 93% and dielectric constant of 1280 was measured.

Fig. 3 shows CTE curves for pure and additives containing $BaTiO_3$. The cubic-tetragonal transformation and the corresponding change in the relative expansion at a temperature close to 130 °C, which is observed for pure $BaTiO_3$, is absent for HDK[C]. Therefore, the calculated values of CTE (100–400 °C) for additives containing $BaTiO_3$ are higher than those for pure $BaTiO_3$ as listed in Table 1.

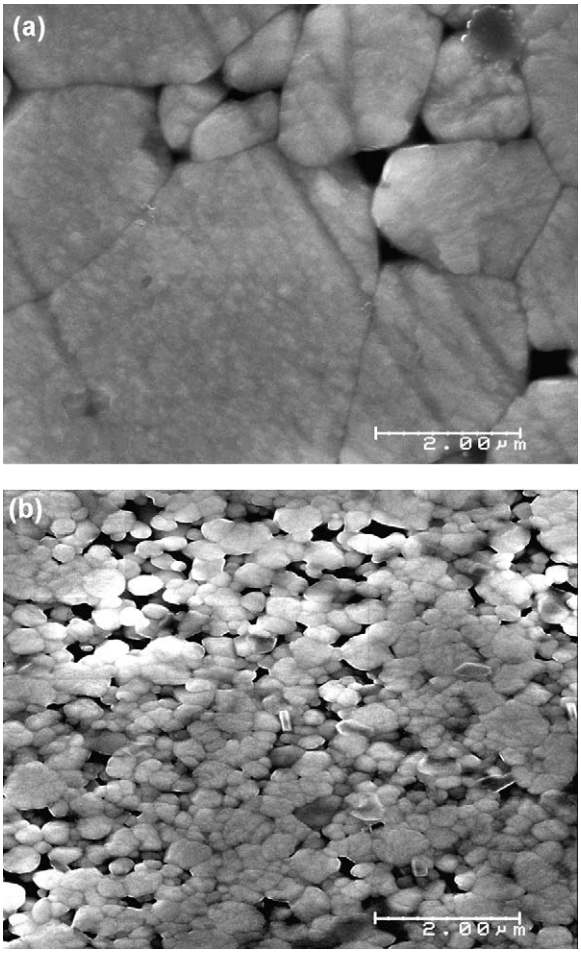

Fig. 4. SEM micrographs of (a) HDK[A] and (b) HDK[C] ceramics sintered at 900 °C.

SEM analysis of HDK[A] ceramic revealed a non-uniform distribution of grain sizes with partially very large grains (Fig. 4a). In contrast, SEM micrograph of HDK[C] ceramic showed a uniform distribution of grain sizes with average grain size of about 0.7 μm as shown in Fig. 4b.

TEM micrograph of HDK[C] shows the ferroelectric domain structure in the core part of the many grains surrounded by a featureless area called 'shell' (Fig. 5). The shell is paraelectric and free from domain wall contrast. The shell region forms as a result of the substitution of additive ions into the $BaTiO_3$ structure.[11] As expected, the concentration of additive ions such as niobium, cobalt and zinc in the shell is much higher than in the core as shown in the EDX analysis of a $BaTiO_3$ crystal with core–shell structure (Fig. 6). This observation is consistent in all core–shell regions. The small EDX counts of additive ions in the core (Fig. 6b) are probably caused by the underlying shell region. This 'core–shell' structure has a significant effect on the dielectric properties of the materials especially on temperature dependency of the dielectric constant. The residual glassy phase is located at triple-grain junctions as shown in Fig. 7. EDX

Fig. 5. TEM micrograph of HDK[C] ceramic showing the core–shell structure.

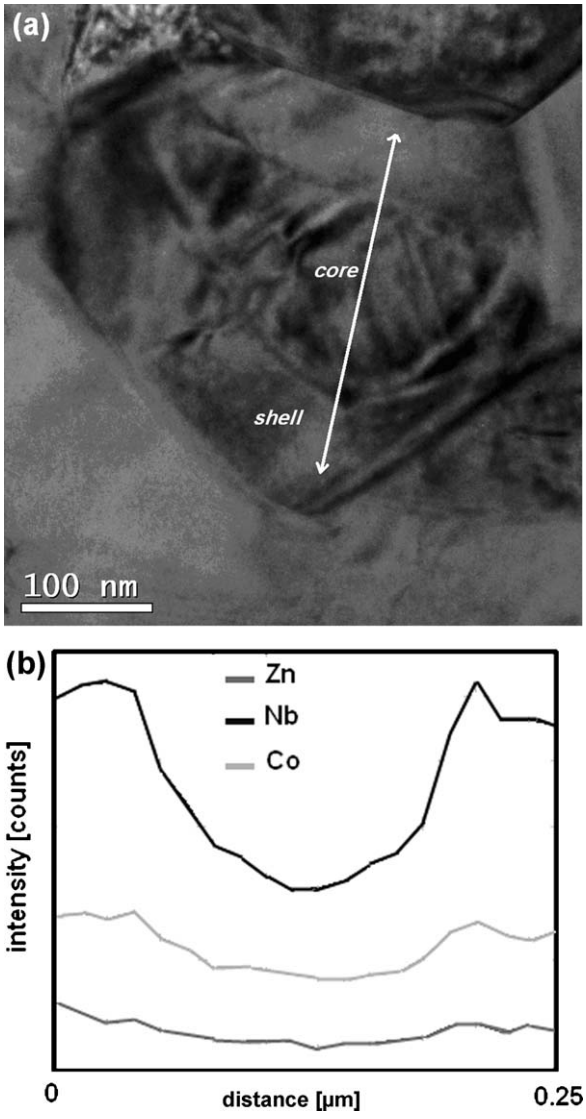

Fig. 6. TEM micrograph of HDK[C] ceramic (a) and the corresponding EDX analysis of niobium, cobalt and zinc (b).

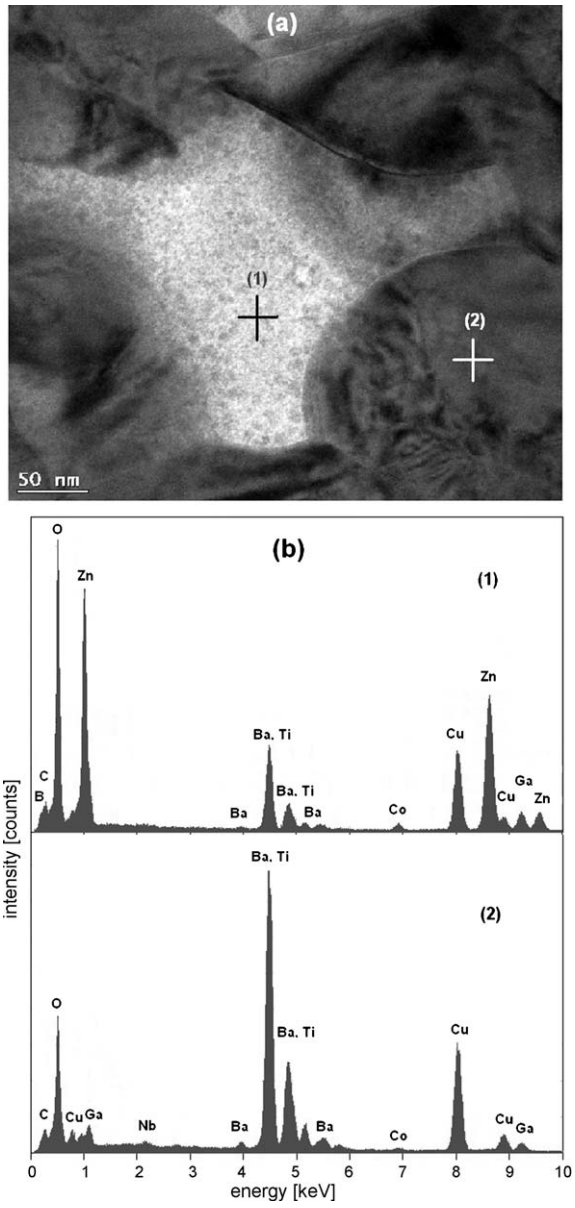

Fig. 7. TEM micrograph from a triple-grain junction of HDK[C] (a) and the corresponding EDX spectra for triple-grain junction (1b) and $BaTiO_3$ grain (2b); Cu and Ga peaks are artefacts of sample preparation and support grid, respectively.

spectrum obtained from a triple-grain junction reveals the high concentration of additives such as Zn, B and Co (Fig. 7b).

TEM micrograph of HDK[A] is shown in Fig. 8. The core–shell structure is observed only in a few grains of HDK[A], with comparatively small core area. The core–shell structure can be also demonstrated by the EDX mapping of niobium in Fig. 9. The higher concentration of niobium in the grain boundary areas of some grains exhibits the shell-structure for these grains. In some other large grains, however, a uniform distribution of niobium is observed. Cobalt ions are mostly located in triple-grain junctions, where the residual flux with a high concentration of zinc is detectable. The element mapping of barium and zinc exhibits the presence of barium ions in the border areas of zinc-rich flux. It is assumed that during liquid phase sintering $BaTiO_3$ particles dissolve completely or partially into the liquid phase. After saturation of the melt with $BaTiO_3$, the reprecipitation process starts. During reprecipitation process the undissolved $BaTiO_3$ particles grow by precipitation of perovskite contained

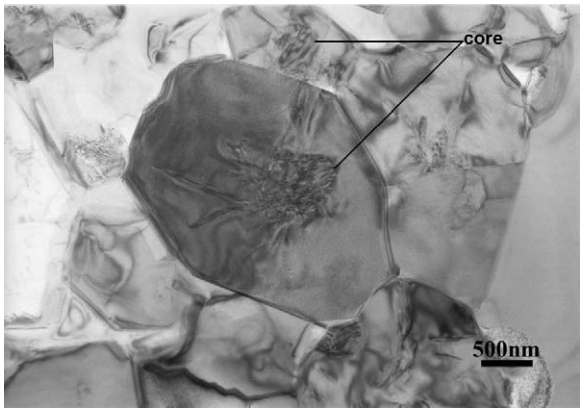

Fig. 8. TEM micrograph of HDK[A] ceramic.

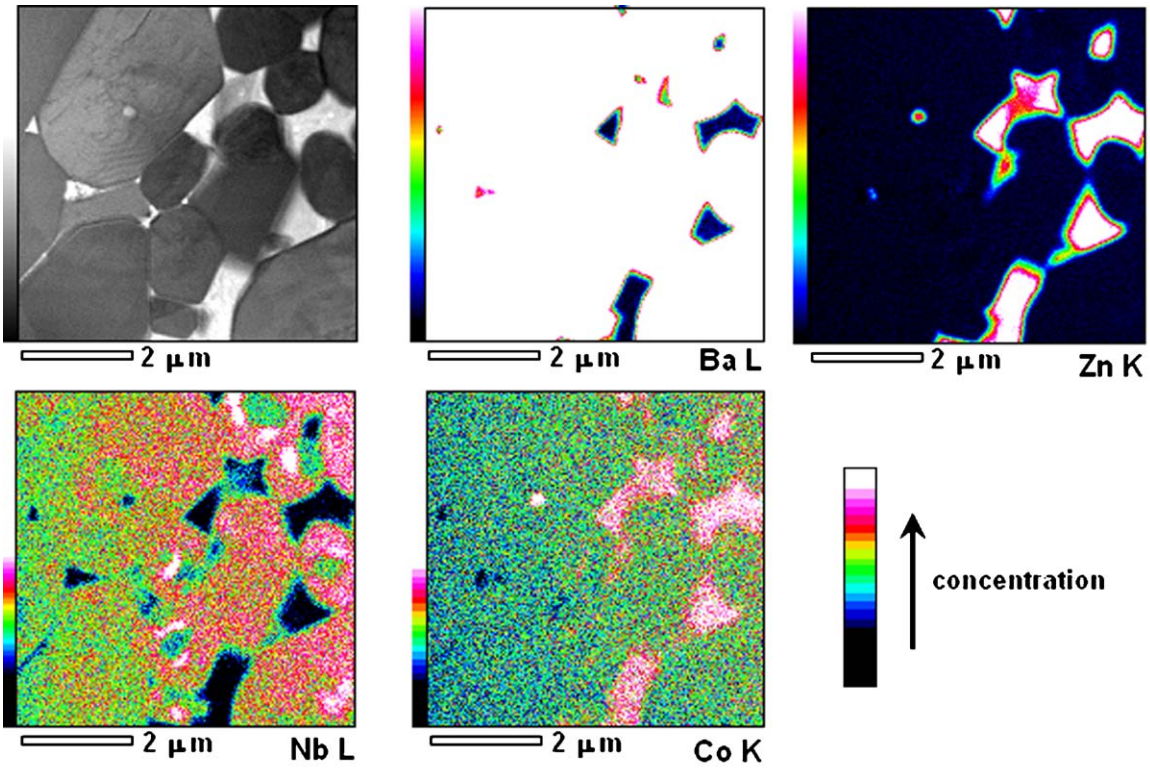

Fig. 9. EDX mapping of elemental distribution of niobium, cobalt, zinc and barium in HDK[A].

additives from the melt and form the core–shell structures.[12] The larger grains with uniform distribution of niobium, on the other hand, are additive containing perovskite which precipitate directly from the melt. The high proportion of these large grains in HDK[A] shows that many $BaTiO_3$ particles dissolved completely into the melt during solution-reprecipitation process which means that a strong interaction between $BaTiO_3$ particles and the ($ZnO–B_2O_3–Li_2O–Nb_2O_5–Co_2O_3$)-additives in HDK[A] occurred.

The XRD patterns of sintered specimens are shown in Fig. 10. The crystalline phase of pure $BaTiO_3$ at room temperature is tetragonal. As shown in the XRD pattern of pure $BaTiO_3$, the characteristic peak splitting of the (2 0 0)/(0 0 2) reflections, which indicates a tetragonal phase, is observed. Additives containing $BaTiO_3$ ceramics do not exhibit this characteristic peak splitting, indicating suppression of the tetragonal structure in favour of a cubic modification of $BaTiO_3$. This observation agrees well with the CTE results.

For the absence of tetragonal phase of the $BaTiO_3$-core in the XRD pattern of additives containing $BaTiO_3$ ceramics, it is assumed that the lattice of the tetragonal core of the grain is distorted into a pseudo-cubic structure by stresses imposed by the cubic shell.[13] Hence, the main crystal phase in the XRD pattern of additives containing $BaTiO_3$ is the cubic phase.

Despite the presence of the sintering additives no formation of new crystalline phases was observed in the XRD-analysis of additives containing $BaTiO_3$ ceramics. This observation approves the TEM evidences, which showed that during liquid phase sintering additives are incorporated into the perovskite or as a residual glassy phase located at triple points.

Fig. 11 illustrates the temperature dependence of the dielectric constant for pure and additives containing $BaTiO_3$ ceramics. The value of the ferroelectric Curie temperature (T_c) for additives containing samples is much lower than that for pure $BaTiO_3$ which is about 130 °C and the dielectric constant exhibits a broadened and diffuse ferroelectric–paraelectric phase transition for additives containing samples. It is supposed that the substitution of titanium by niobium, cobalt and zinc in the shell regions of $BaTiO_3$ grains is responsible for this behaviour.[7,14] The temperature dependence of the dielectric constant decreases

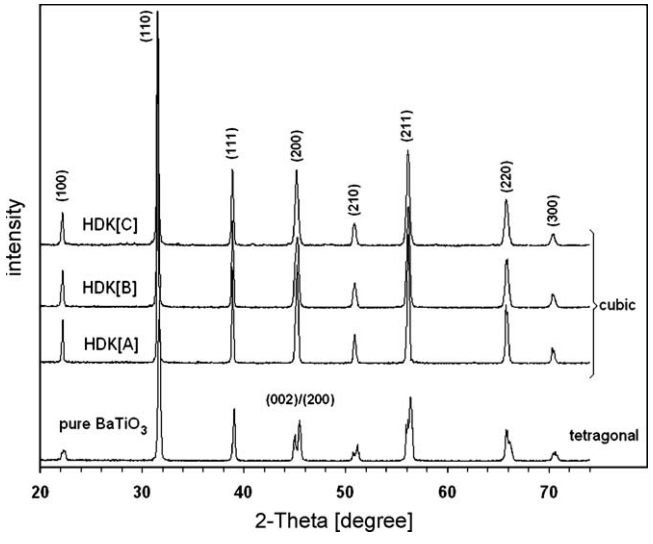

Fig. 10. XRD patterns for pure and additives containing $BaTiO_3$ ceramics.

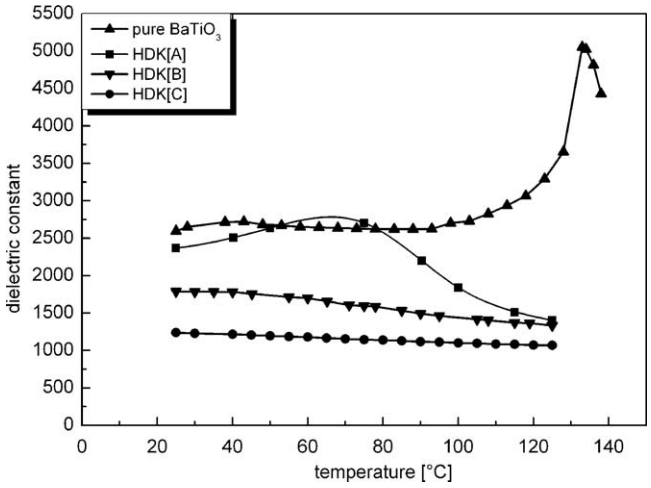

Fig. 11. Temperature dependence of the dielectric constant for pure and additives containing $BaTiO_3$.

when the B_2O_3-content is reduced in the $ZnO–B_2O_3–Li_2O$ flux system from HDK[A] to HDK[B] to HDK[C]. The temperature coefficient of capacitance (TCC) for HDK[C] in the measured temperature range between -40 °C and 125 °C fits well into the X7R specification, i.e., capacitance change of $\leq\pm15\%$ over the temperature range of −55 °C to 125 °C (Fig. 12). The formation of the 'core–shell' structure in a fine-grained microstructure of sample HDK[C] causes the low TCC in this material.[11,15] In contrast to that, a strong grain growth during sintering in HDK[A] causes the higher TCC.

Fig. 13a shows a cross-section of multilayer capacitors of HDK[C] co-fired with pure Ag-electrodes at 900 °C. No delaminations or cracks are observed in the silver/ceramic interfaces. The microprobe element analysis of silver in Fig. 13b shows no evidence of any interfacial reaction between the dielectric layer and the Ag-electrode or Ag-diffusion in the dielectric layer.

The properties of HDK[A] and HDK[C] laminated tapes (without inner electrodes) compared to uniaxially pressed samples of the same materials sintered at 900 °C are listed in Table 2. The densification of the laminates after sintering at 900 °C is higher than pressed samples. Higher densification of the laminates in comparison with pressed samples is probably because of the higher green density and better homogeneity of the green tapes due to about 20 h additionally preparation time of the powders in organics during slurry manufacturing for tape casting. The higher densification of sintered laminates causes the higher dielectric constants and lower dielectric losses compared to pressed samples of the same material. HDK[A]-laminates show a high dielectric constant (ε_r) of about 3000 at 25 °C and a dielectric loss (tan δ) of about 0.024. The dielectric constant and the dielectric loss for HDK[C]-laminates are 1600 and 0.015, respectively.

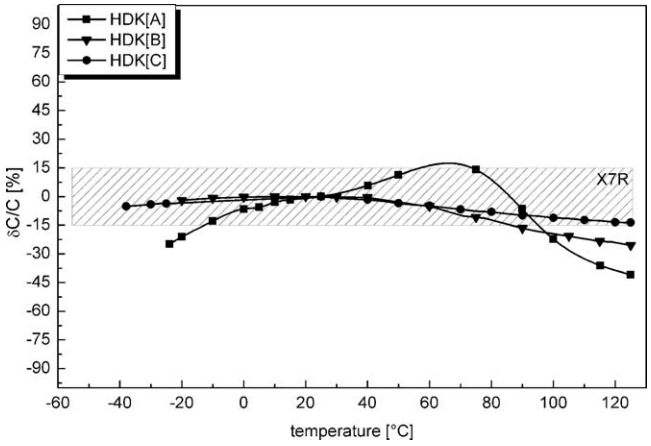

Fig. 12. TCC for additives containing $BaTiO_3$ sintered at 900 °C.

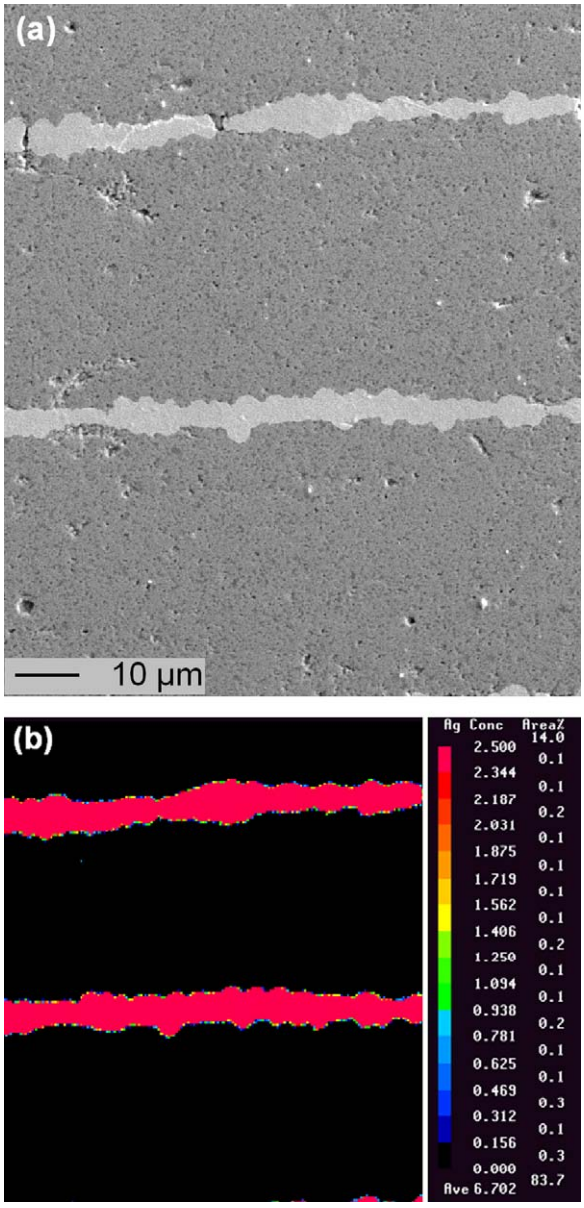

Fig. 13. The cross-section of HDK[C]-multilayer capacitor co-fired with Ag inner electrodes (a) and the corresponding microprobe analysis of silver (b).

Fig. 14 illustrates the TCC for HDK[A]- and HDK[C]-laminates compared to pressed samples of the same material in the temperature range between −20 °C and 125 °C. The results of TCC for uniaxially pressed samples can be quite well reproduced in laminates.

Table 2
Properties of additive containing $BaTiO_3$ ceramics as pressed samples and as laminated tapes.

Samples	Sintering temperature [°C]	Uniaxially pressed samples/Laminated tapes				
		Bulk density [g/cm^3]	Open porosity [%]	Densification [% of theor. density]	ε_r (25 °C, 1 kHz)	tan δ ($\times 10^{-3}$) (25 °C, 1 kHz)
HDK[A]	900	5.67/5.73	0.8/0	98/99	2370/3000	30/24
HDK[C]	900	5.27/5.69	5.0/0.8	93/98.5	1280/1600	30/15

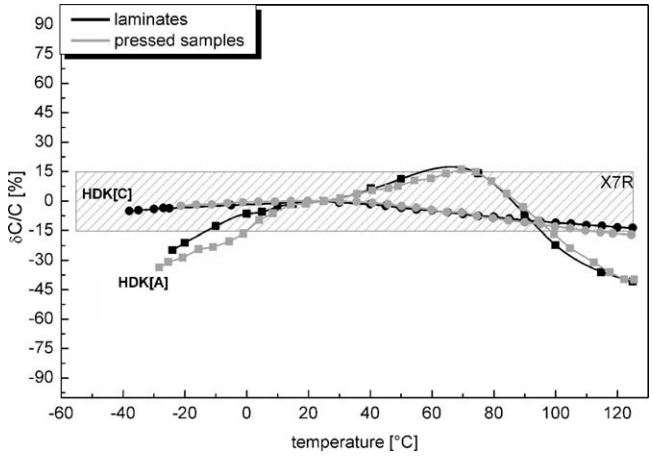

Fig. 14. TCC for laminates and uniaxially pressed samples of HDK[A] and HDK[C] sintered at 900 °C.

Fig. 15 shows the effect of frequency on the capacitance and the dielectric loss for HDK[A] and HDK[C] capacitors. The capacitance decreases slightly over the investigated frequency range (10^3 to 10^6 Hz) while the dielectric loss increases slowly. The HDK[A] and HDK[C] capacitors are applicable at frequencies up to 10^6 Hz because of very low capacitance change in this frequency range.

The breakdown strength is an important parameter for high-voltage capacitors. It is well known that the dielectric breakdown phenomenon of dielectrics is structure-sensitive, and breakdown strength values scatter widely according to the characteristics of the microstructure and thickness of dielectric materials.[16] Thin capacitor tapes are normally used for the capacitor manufacturing, therefore the breakdown strength was measured on thin capacitor tapes with co-fired silver electrodes. The dc dielectric strength of sintered HDK[A] tapes with a thickness of about 105 μm is 14 kV/mm and the dc dielectric strength of sintered HDK[C] tapes with a thickness of about 115 μm amounts to 8 kV/mm. The high dielectric strength of both materials indicates that flux addition has no significant influence on deterioration of breakdown strength. The lower dielectric strength of HDK[C] is probably because of higher porosity (discharge breakdown[17]) of this material compared to HDK[A] (Table 2).

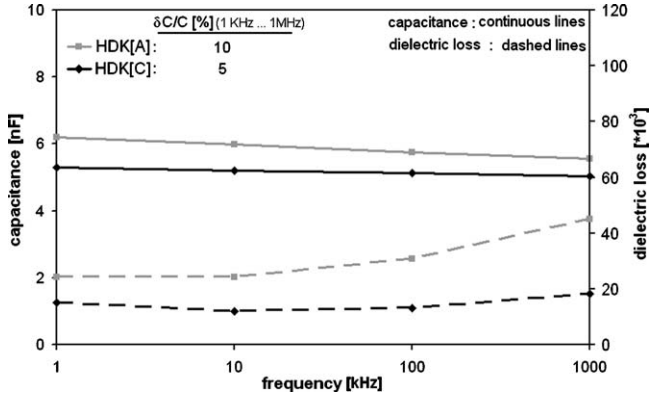

Fig. 15. Frequency dependence of the capacitance (continuous lines) and the dielectric loss (dashed lines) for HDK[A] and HDK[C] ceramics measured at room temperature.

4. Conclusions

An addition of $ZnO–B_2O_3–Li_2O–Nb_2O_5–Co_2O_3$ compositions to $BaTiO_3$ lowered the sintering temperature to 900 °C. The material can be fully densified after sintering at 900 °C for 2 h. The dielectric properties were found to strongly depend on the composition of $ZnO–B_2O_3–Li_2O$ flux system. By increasing of B_2O_3 content in the $ZnO–B_2O_3–Li_2O$ flux system the dielectric constant at room temperature decreases, but the temperature stability of the dielectric constant improves considerably. The newly developed capacitor materials exhibit the dielectric constant up to 3000 and the dielectric loss less than 0.024.

Excellent densification without any interfacial reaction between the dielectric layers and the Ag-electrode was obtained in multilayer capacitors sintered at 900 °C, which is promising for integration of buried capacitors into LTCC substrate.

Acknowledgements

The authors would like to thank Mr. Schadrack (dilatometer measurements), Mrs. Oder, Mrs. Benemann, Mrs. Strauß (REM, EDX und WDX analyses), Dr. Doerfel, Mrs. Rooch (FIB and TEM) all from BAM and Mr. Moerbe (dielectric measurements) from Friwo Mobile GmbH.

References

1. Sebastian1 MT, Jantunen H. Low loss dielectric materials for LTCC applications: a review. *Int Mater Rev* 2008;**53**(2):57–90.
2. Prakash D, Sharma BP, Rama Mohan TR, Gopalan P. Flux additions in barium titanate: overview and prospects. *J Solid State Chem* 2000;**155**:86–95.
3. Desgardin G, Haussonne JM. $BaLiF_3$—a new sintering agent for $BaTiO_3$-based capacitors. *J Am Ceram Soc Bull* 1985;**64**(4):564–70.
4. Naghib zadeh H, Giltzky C, Doerfel I, Rabe T. Low temperature sintering of barium titanate ceramics assisted by addition of lithium fluoride-containing sintering additives. *J Eur Ceram Soc* 2010;**30**:81–6.
5. Valant M, Suvorov D, Pullar RC, Sarma K, Alford NMCN. A mechanism for low-temperature sintering. *J Eur Ceram Soc* 2006;**26**:2777–83.

6. Hsiang HI, Hsi CS, Huang CC, Fu SL. Low temperature sintering and dielectric properties of $BaTiO_3$ with glass addition. *Mater Chem Phys* 2009;**113**:658–63.
7. Du M, Li Y, Yuan Y, Zhang S, Tang B. A novel approach to $BaTiO_3$-based X8R ceramics by calcium borosilicate glass ceramic doping. *J Electron Mater* 2007;**36**(10):1389–94.
8. Ian Burn. Flux-sintered $BaTiO_3$ dielectrics. *J Mater Sci* 1982;**17**:1398–408.
9. Song TH, Randall CA. Copper cofire X7R dielectrics and multilayer capacitors based on zinc borate fluxed barium titanate ceramic. *J Electroceram* 2003;**10**:39–46.
10. Armstrong TR, Young KA, Buchanan RC. Dielectric properties of fluxed barium titanate ceramics with zirconia additions. *J Am Ceram Soc* 1990;**73**(3):700–6.
11. Hennings D, Schreinemacher BS. Temperature-stable dielectric materials in the system $BaTiO_3$–Nb_2O_5–Co_3O_4. *J Eur Ceram Soc* 1994;**14**:463–71.
12. Hennings D, Rosenstein G. Temperature-stable dielectrics based on chemically inhomogeneous $BaTiO_3$. *J Am Ceram Soc* 1984;**67**(4): 249–55.
13. Armstrong TR, Buchanan RC. Influence of core–shell grains on the internal stress state and permittivity response of zirconia-modified barium titanate. *J Am Ceram Soc* 1990;**73**(5):1268–73.
14. Subbarao EC, Shirane G. Dielectric and structural studies in the systems $Ba(Ti,Nb)O_3$ and $Ba(Ti,Ta)O_3$. *J Am Ceram Soc* 1959;**42**:279–84.
15. Arlt G, Hennings D, DeWith G. Dielectric properties of fine-grained barium titanate. *J Appl Phys* 1985;**58**:1619–25.
16. Schomann KD. Zum elektrischen Durchschlag von keramischem Bariumtitanat und Barium–Strontium–Titanat. *Arch Elektrotech* 1974;**56**: 223–7.
17. Moulson AJ, Herbert JM. *Electroceramics*. 2nd ed. Chichester, West Sussex: John Wiley & Sons Ltd.; 2003.